Impact of Antenna Coupling on Diversity Performance: Complete Network Theory Analysis

Jon W. Wallace and Michael A. Jensen
Department of Electrical and Computer Engineering
Brigham Young University, 459 CB, Provo, UT 84602-4099
Phone: (801) 422-5736 Fax: (801) 422-0201
Email: wall@ieee.org, jensen@ee.byu.edu

***Abstract*— In antenna diversity systems, mutual coupling of closely-spaced antennas alters the element radiation and impedance properties, thereby impacting the system diversity performance. Past studies have emphasized the effect of the distorted pattern and largely neglected the effect of altered impedance (and therefore receive signal-to-noise ratio) on the diversity behavior. Here, we present a new network analysis which facilitates a complete characterization of the system and comparison of diversity performance for various impedance terminations. Representative results reveal that for closely-spaced antennas, the termination can play a noticeable role in determining the diversity gain offered by coupled antennas.**

I. Introduction

Antenna arrays play a crucial role in wireless communications over multipath fading channels, with antenna diversity being the topic of considerable research for many decades [1]. When using multiple antenna elements for diversity implementation on small personal communications devices, mutual coupling between the closely-spaced antenna elements alters both their terminal impedance and radiation pattern characteristics. Past studies on the impact of this coupling on diversity performance emphasize the influence of distorted element radiation pattern [2]-[6] and neglect the effect of the altered impedance on the received power. Even when this latter effect is included, typically only a single termination [7], [8] or a limited set of terminations [9] is considered.

In this paper, we present a network theory analysis of coupled diversity antenna systems that includes the impact of both radiation pattern and antenna termination. This framework allows comparison of the diversity performance for different terminations, including an optimal multi-port conjugate match. The analysis shows that this optimal match not only maximizes power to the load, but also perfectly decorrelates the received branch signals. Computational results for mutually-coupled dipoles demonstrate the achievable diversity performance for different antenna terminations. These results indicate that for close spacing, the termination can play a key role in the achievable system diversity performance.

II. Coupled Antenna Network Representation

A. S-Parameter Network Description

For high frequency systems such as mutually-coupled antenna networks, the S-parameter matrix representation [10] provides a convenient analysis framework. In this description, the voltages and currents on each of the N ports are decomposed into inward ($\overline{a}$) and outward ($\overline{b}$) traveling waves that satisfy the relation $\overline{b} = \overline{\overline{S}}\,\overline{a}$, where $\overline{\overline{S}}$ is the $N\times N$ S-parameter matrix or S-matrix. The voltage on (v_n) and current into (i_n) the nth port are related to a_n and b_n according to

$$v_n = Z_0^{1/2}(a_n + b_n) \qquad i_n = Z_0^{-1/2}(a_n - b_n), \tag{1}$$

where Z_0 is a normalizing impedance.

Consider now the network depiction of the coupled receiving antenna system shown in Figure 1. In this diagram, each element of the coupled array is characterized by a generator whose signal passes through a coupling matrix $\overline{\overline{S}}_c$ with a block representation

$$\overline{\overline{S}}_c = \begin{bmatrix} \overline{\overline{S}}_{c,11} & \overline{\overline{S}}_{c,12} \\ \overline{\overline{S}}_{c,21} & \overline{\overline{S}}_{c,22} = \overline{\overline{S}}_S \end{bmatrix}, \tag{2}$$

where 1 and 2 refer to input and output ports respectively. Here, we have used the notation $\overline{\overline{S}}_{c,22} = \overline{\overline{S}}_S$ to emphasize that this block represents the traditional "source termination" encountered in S-parameter circuit analysis. It is also noteworthy that $\overline{\overline{S}}_S$ is the coupled S-parameter matrix measured at the antenna element input ports. Rather than try to characterize the remaining blocks of $\overline{\overline{S}}_c$, we will simply represent the excitation signal at the antenna ports as $\overline{b}_S$ so that

$$\overline{a}_1 = \overline{\overline{S}}_S\overline{b}_1 + \overline{b}_S. \tag{3}$$

The N-port antenna in Figure 1 is attached to the M-port load network $\overline{\overline{S}}_L$ through a matching network with S-parameter matrix $\overline{\overline{S}}_M$ consisting of blocks $\overline{\overline{S}}_{ij}$, $i,j \in 1,2$ arranged in a form similar to that in (2). Here, we will consider networks having the same number of input and output ports ($M = N$). The input reflection coefficient which will be used in later analysis can be expressed as

$$\overline{\overline{\Gamma}}_{\text{in}} = \overline{\overline{S}}_{11} + \overline{\overline{S}}_{12}(\overline{\overline{I}} - \overline{\overline{S}}_L\overline{\overline{S}}_{22})^{-1}\overline{\overline{S}}_L\overline{\overline{S}}_{21}. \tag{4}$$

B. Lossless Matching Networks

Lossless, passive matching networks are of particular interest since they exhibit low noise figures. Such networks must satisfy $\overline{\overline{S}}_M^H\overline{\overline{S}}_M = \overline{\overline{I}}$, leading to relationships between the sub-blocks $\overline{\overline{S}}_{ij}$. Substitution of the singular value decomposition

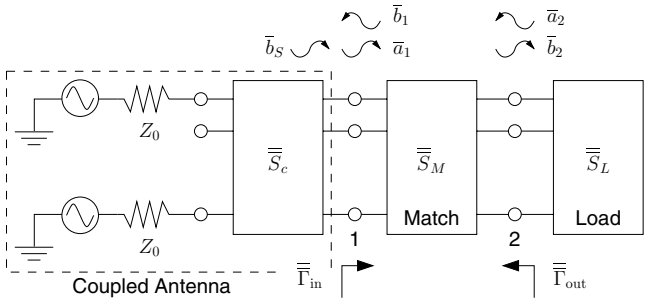

Fig. 1. System model of a coupled diversity antenna array connected to a multiport matching circuit and individual loads.

(SVD) of these sub-blocks $\overline{\overline{S}}_{ij} = \overline{\overline{U}}_{ij}\overline{\overline{\Lambda}}_{ij}^{1/2}\overline{\overline{V}}_{ij}^{H}$ yields the constraints

$$\begin{aligned} \overline{\overline{V}}_{21}\overline{\overline{\Theta}}_{21} &= \overline{\overline{V}}_{11} \qquad & \overline{\overline{\Lambda}}_{21} &= \overline{\overline{I}} - \overline{\overline{\Lambda}}_{11} \\ \overline{\overline{V}}_{12}\overline{\overline{\Theta}}_{12} &= \overline{\overline{V}}_{22} \qquad & \overline{\overline{\Lambda}}_{12} &= \overline{\overline{I}} - \overline{\overline{\Lambda}}_{22}, \end{aligned} \tag{5}$$

where $\overline{\overline{\Theta}}_{21}$ and $\overline{\overline{\Theta}}_{12}$ are diagonal *phase shift* matrices with arbitrary complex elements of unit magnitude.

III. Diversity Performance

A. Received Signal Covariance

The performance of antenna diversity systems depends upon the signal strength on each antenna branch as well as the signal correlation between branches. To assess these metrics for different degrees of antenna coupling and receiver terminations, we will compute the covariance matrix for the voltages received on each branch. For the network in Figure 1 with $Z_0 = 1$, the received voltages are given by

$$\overline{v}_L = \overline{b}_2 + \overline{a}_2 = (\overline{\overline{I}} + \overline{\overline{S}}_L)(\overline{\overline{I}} - \overline{\overline{S}}_{22}\overline{\overline{S}}_L)^{-1}\overline{\overline{S}}_{21}\overline{a}_1 \tag{6}$$

where we have used that $\overline{b}_2 = \overline{\overline{S}}_{22}\overline{a}_2 + \overline{\overline{S}}_{21}\overline{a}_1$ and $\overline{a}_2 = \overline{\overline{S}}_L\overline{b}_2$. Using (3) with $\overline{b}_1 = \overline{\overline{\Gamma}}_{\rm in}\overline{a}_1$ in (6) leads to

$$\overline{v}_L = \underbrace{(\overline{\overline{I}} + \overline{\overline{S}}_L)(\overline{\overline{I}} - \overline{\overline{S}}_{22}\overline{\overline{S}}_L)^{-1}\overline{\overline{S}}_{21}(\overline{\overline{I}} - \overline{\overline{S}}_S\overline{\overline{\Gamma}}_{\rm in})^{-1}}_{\overline{\overline{Q}}}\,\overline{b}_S. \tag{7}$$

The covariance matrix is therefore given as $\overline{\overline{R}}_L = \mathrm{E}\{\overline{v}_L\overline{v}_L^H\} = \overline{\overline{Q}}\;\overline{\overline{R}}_S\overline{\overline{Q}}^H$, where $\overline{\overline{R}}_S = \mathrm{E}\{\overline{b}_S\overline{b}_S^H\}$ is the covariance of $\overline{b}_S$ and $\mathrm{E}\{\cdot\}$ represents an expectation.

To relate $\overline{b}_S$ to the physical antenna properties, consider an antenna array consisting of N arbitrary antenna elements embedded in a reciprocal medium. The far-field radiation pattern of the array is

$$\overline{E}(\Omega) = \sum_n \overline{F}_n(\Omega)\; i_n = \overline{\overline{F}}(\Omega)\;\overline{i}, \tag{8}$$

where i_n is the current on the nth element, $\overline{F}_n(\Omega)$ is the vector far-field radiation pattern of the nth element when all other elements are open-circuited ($i_k = 0$ for $k \neq n$), and Ω represents a direction in solid angle. $\overline{\overline{F}}(\Omega)$ represents all of the far-field patterns (one per column) stacked into a single matrix.

Now, assume a plane wave arrives from the solid angle direction Ω_0 with complex field strength $E_0 = A\exp(j\phi)$ (A real) and electric field polarization vector $\hat{e}$. If the antennas are open-circuited, then by reciprocity the voltages on the antenna elements are given by

$$\overline{v} = 2\;c_1 E_0\overline{\overline{F}}(\Omega_0)^T\hat{e}, \tag{9}$$

where c_1 is a complex constant. Equating this response to the voltage obtained assuming that port 1 in Figure 1 is open-circuited, we arrive at the expression

$$\overline{b}_S = c_1 E_0(\overline{\overline{I}} - \overline{\overline{S}}_S)\overline{\overline{F}}(\Omega_0)^T\hat{e} = c_1 E_0\overline{\overline{F}}'(\Omega_0)^T\hat{e} \tag{10}$$

where we have included the impedance mismatch factor $(\overline{\overline{I}} - \overline{\overline{S}}_S)$ in the effective radiation pattern $\overline{\overline{F}}'(\Omega_0)$.

The covariance of $\overline{b}_S$ may now be written explicitly as

$$\overline{\overline{R}}_S = |c_1|^2\int d\Omega\; d\hat{e}\; dA\; p(\Omega,\hat{e},A)A^2\overline{\overline{F}}'(\Omega)^T\hat{e}\,\hat{e}^T\overline{\overline{F}}'^*(\Omega) \tag{11}$$

where $p(\Omega,\hat{e},A)$ represents the probability density of the incident field angle of arrival, polarization, and amplitude. For the following, we make the common assumptions that: 1) the antennas and incident waves have the same single polarization, 2) arrival angles are restricted to and uniformly distributed on a solid angle sector $\Delta\Omega$, and 3) field amplitudes are independent of arrival angle and have a variance E^2. Under these contraints, we have

$$\overline{\overline{R}}_S^* = |c_1|^2E^2\frac{\int_{\Delta\Omega}d\Omega\;\overline{\overline{F}}'^H(\Omega)\overline{\overline{F}}'(\Omega)}{\int_{\Delta\Omega}d\Omega} = c_2\overline{\overline{P}}, \tag{12}$$

where $c_2 = (|c_1|^2E^2)/\int_{\Delta\Omega}d\Omega$. The covariance of $\overline{b}_L$ can now be written as

$$\overline{\overline{R}}_L = c_2\overline{\overline{Q}}\;\overline{\overline{P}}^*\overline{\overline{Q}}^H. \tag{13}$$

Sometimes a more descriptive model of the channel is available (such as a path-based model [11]). In this case, $\overline{b}_S$ can be computed from (10), with E_0 and $\hat{e}$ obtained from the model, for a set of Monte Carlo channel realizations. The covariance $\overline{\overline{R}}_S = \mathrm{E}\{\overline{b}_S\overline{b}_S^H\}$ can then be constructed using a sample mean to estimate the expectation.

B. Source Covariance for Full Angular Spread

Under the special case that the multipath arrival sector $\Delta\Omega$ extends over the full angular range of the propagation environment, a simplification can be introduced. For the array operating as a transmitter, the power radiated by the array is given as

$$P_{\rm rad} = c_3\oint d\Omega\;\|\overline{E}(\Omega)\|^2 = c_3\overline{a}^H\overline{\overline{P}}\overline{a} \tag{14}$$

where c_3 is a real constant and we have used (1) and (8).

For a lossless antenna, the power radiated is equal to the power delivered to the antenna network $P_{\rm net} = \|\overline{a}\|^2 - \|\overline{b}\|^2 = \overline{a}^H\left(\overline{\overline{I}} - \overline{\overline{S}}^H\overline{\overline{S}}\right)\overline{a}$. Equating (14) to this expression and using (12) leads to the source covariance

$$\overline{\overline{R}}_S = c_2\overline{\overline{P}}^* = c(\overline{\overline{I}} - \overline{\overline{S}}_S^H\overline{\overline{S}}_S)^* = c(\overline{\overline{I}} - \overline{\overline{S}}_S\overline{\overline{S}}_S^H), \tag{15}$$

where $c = c_2/c_3$ and the last equality stems from assuming that the antenna and transmission media are reciprocal ($\overline{\overline{S}}_S = \overline{\overline{S}}_S^T$). The key observation concerning (15) is that under the propagation conditions outlined, the covariance matrix can be computed without resorting to integration of the radiation patterns, as previously observed in [8].

C. Simplifications for Practical Terminations

This section shows how the general equations for the covariance matrix is simplified for several practical terminations. For all cases except for open-circuited terminations, we use the (realistic) load network consisting of one resistor of value $Z_0 = 1$ on each port, leading to $\overline{\overline{S}}_L = \overline{\overline{0}}$. Since this results in $\overline{\overline{\Gamma}}_{\rm in} = \overline{\overline{S}}_{11}$, the matching network is used to create the desired antenna port terminations.

Open-Circuit Terminations: For open-circuit termination, the matching network is removed ($\overline{\overline{S}}_{11} = \overline{\overline{S}}_{22} = 0$, $\overline{\overline{S}}_{12} = \overline{\overline{S}}_{21} = \overline{\overline{I}}$) such that $\overline{\overline{\Gamma}}_{\rm in} = \overline{\overline{S}}_L = \overline{\overline{I}}$. Under these conditions, the covariance matrix simplifies to

$$\overline{\overline{R}}_{L,\rm oc} = 4(\overline{\overline{I}} - \overline{\overline{S}}_S)^{-1}\overline{\overline{R}}_S(\overline{\overline{I}} - \overline{\overline{S}}_S^H)^{-1}. \quad (16)$$

Characteristic Impedance Terminations: In this case, we again remove the matching network but use $\overline{\overline{\Gamma}}_{\rm in} = \overline{\overline{0}}$. This results in $\overline{\overline{Q}} = \overline{\overline{I}}$ such that

$$\overline{\overline{R}}_{L,Z_0} = \overline{\overline{R}}_S. \quad (17)$$

Self-Impedance Match: Self-impedance match refers to the condition where port n is terminated in the self-impedance of antenna n. In this case, $\overline{\overline{\Gamma}}_{\rm in} = \overline{\overline{S}}_{11} = \mathrm{diag}\{\overline{\overline{S}}_S^*\}$, where the $\mathrm{diag}\{\cdot\}$ operator creates a diagonal matrix from the diagonal entries of the operand. The resulting covariance matrix becomes

$$\overline{\overline{R}}_{L,\rm self} = \overline{\overline{S}}_{21}(\overline{\overline{I}} - \overline{\overline{S}}_S\overline{\overline{S}}_{11})^{-1}\overline{\overline{R}}_S(\overline{\overline{I}} - \overline{\overline{S}}_S\overline{\overline{S}}_{11})^{H(-1)}\overline{\overline{S}}_{21}^H. \quad (18)$$

D. Optimal Hermitian Match

Maximizing the power transfer to the load requires a multiport conjugate match, which for our network means that $\overline{\overline{S}}_{11} = \overline{\overline{S}}_S^H$ [8]. As a framework for analysis, let $\overline{\overline{\Gamma}}_{\rm in} = \overline{\overline{S}}_{11} = \overline{\overline{S}}_S^H$, which leads to the covariance matrix

$$\overline{\overline{R}}_{L,\rm opt} = \overline{\overline{S}}_{21}(\overline{\overline{I}} - \overline{\overline{S}}_S\overline{\overline{S}}_S^H)^{-1}\overline{\overline{R}}_S(\overline{\overline{I}} - \overline{\overline{S}}_S\overline{\overline{S}}_S^H)^{-1}\overline{\overline{S}}_{21}^H. \quad (19)$$

Using the conditions for lossless matching networks from Section II-B, the two relevant blocks of the matching network are represented using

$$\begin{aligned}\overline{\overline{S}}_{11} &= \overline{\overline{S}}_S^H = \overline{\overline{V}}\,\overline{\overline{\Lambda}}^{1/2}\overline{\overline{U}}^H \\ \overline{\overline{S}}_{21} &= \overline{\overline{U}}_{21}(\overline{\overline{I}} - \overline{\overline{\Lambda}})^{1/2}\overline{\overline{\Theta}}_{21}\overline{\overline{U}}^H.\end{aligned} \quad (20)$$

These conditions transform (19) to the form

$$\begin{aligned}\overline{\overline{R}}_{L,\rm opt} \;=\; & \overline{\overline{U}}_{21}\overline{\overline{\Theta}}_{21}(\overline{\overline{I}} - \overline{\overline{\Lambda}})^{-1/2}\overline{\overline{U}}^H\overline{\overline{R}}_S\overline{\overline{U}} \\ & \times(\overline{\overline{I}} - \overline{\overline{\Lambda}})^{-1/2}\overline{\overline{\Theta}}_{21}^H\overline{\overline{U}}_{21}^H.\end{aligned} \quad (21)$$

Under the conditions considered in Section III-B where multipath components arrive uniformly from all angles of arrival, we use (15) along with (20) to obtain

$$\overline{\overline{R}}_S = c\overline{\overline{U}}(\overline{\overline{I}} - \overline{\overline{\Lambda}})\overline{\overline{U}}^H. \quad (22)$$

Placing this result in (21) yields the simplified expression

$$\overline{\overline{R}}_{L,\rm opt} = c\overline{\overline{U}}_{21}\overline{\overline{\Theta}}_{21}\overline{\overline{\Theta}}_{21}^H\overline{\overline{U}}_{21}^H = c\overline{\overline{I}}. \quad (23)$$

This result implies that under these circumstances, the optimal Hermitian match perfectly decorrelates the signals on the loads. Other studies have noted the reduced correlation associated with termination [2], [9], but have not provided a framework for arriving at this perfectly diagonal covariance. It is important to realize that this decorrelation is simply the result of recombination of the received signals, and therefore does not necessarily enhance the diversity performance of the system. Nevertheless, it is interesting to be able to mathematically predict this behavior using the proposed analysis approach.

When full angular spread does not exist, the optimal matching network can be further specified to diagonalize the covariance matrix. Consider again (21) and let

$$\overline{\overline{T}} = (\overline{\overline{I}} - \overline{\overline{\Lambda}})^{-1/2}\overline{\overline{U}}^H\overline{\overline{R}}_S\overline{\overline{U}}(\overline{\overline{I}} - \overline{\overline{\Lambda}})^{-1/2} = \overline{\overline{U}}_T\overline{\overline{\Lambda}}_T\overline{\overline{U}}_T^H \quad (24)$$

where the last equality represents the eigenvector decomposition (EVD) of $\overline{\overline{T}}$. Since $\overline{\overline{U}}_{21}\overline{\overline{\Theta}}_{21}$ is arbitrary as long as it is unitary, we can choose $\overline{\overline{U}}_{21}\overline{\overline{\Theta}}_{21} = \overline{\overline{U}}_T^H$ to obtain

$$\overline{\overline{R}}_{L,\rm opt} = \overline{\overline{\Lambda}}_T, \quad (25)$$

the diagonal matrix of eigenvalues of $\overline{\overline{T}}$. In the case of two vertically oriented dipoles, the problem symmetry leads to 2×2 real Toeplitz symmetric matrices that share common eigenvectors. The result is that the diagonalization can be accomplished by choosing $\overline{\overline{U}}_{21} = \overline{\overline{I}}$.

IV. Computational Examples

To demonstrate application of the analysis framework developed in this paper and to illustrate the impact of termination on the diversity performance of mutually coupled antennas, we will explore a receive array consisting of two coupled dipoles. While closed-form expressions for coupled dipole impedance matrices exist (for reasonable antenna spacings), expressions for the patterns do not, motivating the use of full-wave electromagnetic solutions. Furthermore, simple thin-wire simulations assume that the current does not vary in azimuth around the wire, an assumption that is violated for very closely-spaced dipoles [12] leading to inaccurate impedance calculations.

In this work, it is desired to characterize the coupled antennas as the spacing is reduced to zero. As a result, we have chosen to use the finite-difference time-domain (FDTD) method [4] to perform detailed simulations that return both S-parameter and radiation pattern descriptions for the dipole antennas. In this analysis, the z-oriented half-wave (total-length) dipoles with wire radius 0.01λ and separated by a

distance d are located at the center of the computational domain. Because we are considering narrowband systems, single-frequency antenna excitation is used. The FDTD grid uses 80 cells per wavelength in the z direction and 200 cells per wavelength in the x and y directions. This finer resolution is required to adequately model the current variations in the azimuthal direction on the finite-radius wire for close antenna spacings.

Because of the fine grid resolution, a relatively small buffer region of only a quarter wavelength (to minimize simulation memory) is placed between the antennas and the terminating 8-cell perfectly matched layer (PML) absorbing boundary condition (ABC). The impact of this small buffer region was investigated by reducing the x and y resolution to 100 cells per wavelength and comparing impedances and radiation patterns for half- and quarter-wavelength buffer thicknesses with a dipole spacing of 0.13λ. The resulting fractional change in self and mutual impedances was only 1.4×10^{-4} and 1.9×10^{-4}, respectively. The maximum fractional change in the radiated electric field intensity when a single antenna was excited was 1.5×10^{-4}.

Based upon the formulation in Section III-A, pattern computations are performed when one antenna is excited while the second is terminated in an open circuit. The antenna S-parameter matrix $\overline{\overline{S}}_S$ is computed with the antennas terminated in Z_0. Multipath arrivals are assumed confined to the horizontal plane in this study. Unless otherwise specified, arrival angles are uniformly distributed within this plane ($0 \leq \phi < 2\pi$). As a result, the radiation patterns are normalized such that

$$\int_0^{2\pi} P(\theta = \pi/2, \phi)\ d\phi = 1 \tag{26}$$

where $P(\theta, \phi)$ is the antenna power pattern. This same normalization is applied to an array of uncoupled dipoles used as a baseline for quantifying diversity performance.

As a first example, it is interesting to compute the correlation coefficient of the signals on the two antennas. This is simply derived from the covariance matrix using

$$\rho = \frac{R_{L,12}}{\sqrt{R_{L,11} R_{L,22}}}, \tag{27}$$

where $R_{L,ij}$ represents the i, jth element of the computed load covariance matrix. Figure 2 plots the variation of this quantity as a function of antenna spacing for the different terminations considered in this work. For the optimal match, the matrix $\overline{\overline{U}}_{21}$ is chosen as $\overline{\overline{U}}_{11}$ and $\overline{\overline{I}}$ for the cases where $\overline{\overline{R}}_L$ is not diagonal and diagonal, respectively. The reduced correlation afforded by proper termination is clearly apparent in these results. It is noteworthy that all terminations result in reduced correlation as compared with the result obtained for uncoupled dipoles, confirming the results of other research [5], [6], [9]. However, it is important to point out that this study has included the effects of the mutual impedance *and* terminations in the analysis and provides a comprehensive examination of this effect for a variety of termination types.

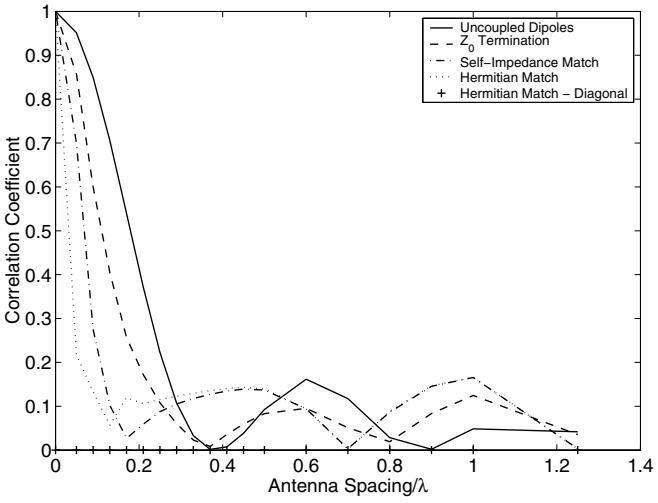

Fig. 2. Plot of branch signal correlation as a function of antenna spacing for two coupled dipole antennas terminated with various loads. The result for independent dipoles is shown for comparison.

The correlation coefficient provides a partial indication of the system diversity performance, since the power on each branch is also an important factor. In order to investigate the full diversity benefit, we utilize the concept of *Effective Diversity Order* introduced in [7]. In this metric, the diversity benefit is measured in comparison to what is possible using two equal power and uncoupled antennas. For this study, the diversity order is determined from the data at the 1% level on the diversity cumulative distribution functions and assuming maximal ratio combining. For the coupled antennas, diversity performance is computed using the eigenvalues of the covariance matrix to represent two independent branches with unequal average SNR. Full details on this metric are provided in [7].

Figure 3 shows the diversity order as a function of spacing for the different termination conditions. As can be seen, for small antenna spacings, improved matching leads to improved diversity performance. Most striking is the fact that the optimal matching circuits lead to better performance than what is obtainable with independent, equal power branches for small antenna spacings (characterized as a diversity order > 2). This behavior stems from the fact that optimally matched coupled antennas can capture more power than can be collected by two independent dipoles. One reasonable explanation for this increased effective aperture is that a portion of the power scattered by each receiving antenna can be recaptured by the adjacent antenna. This metric also reveals the expected result that although the matching network can diagonalize the covariance matrix, this diagonalization comes at the expense of unequal branch SNR and therefore does not facilitate additional diversity gain. For this reason, the two Hermitian match results lie on top of each other in the plot. For larger spacings, clearly the match becomes less important, as the curves for the different terminations tend to the same value.

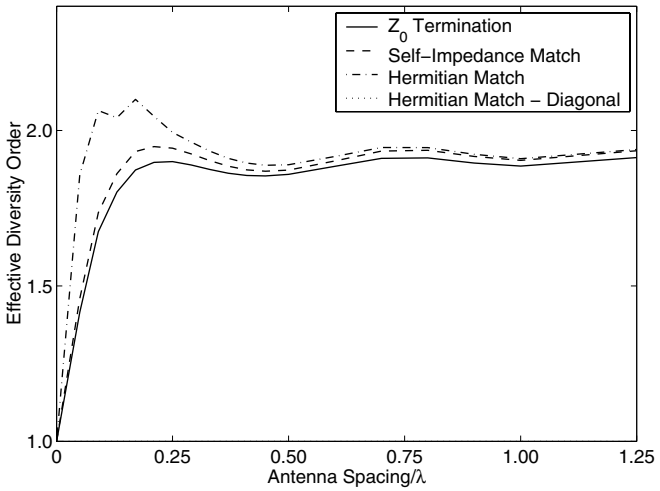

Fig. 3. Plot of effective diversity order as a function of antenna spacing for two coupled dipole antennas terminated with various loads. Correlations are computed assuming arrivals are uniformly distributed within the horizontal plane.

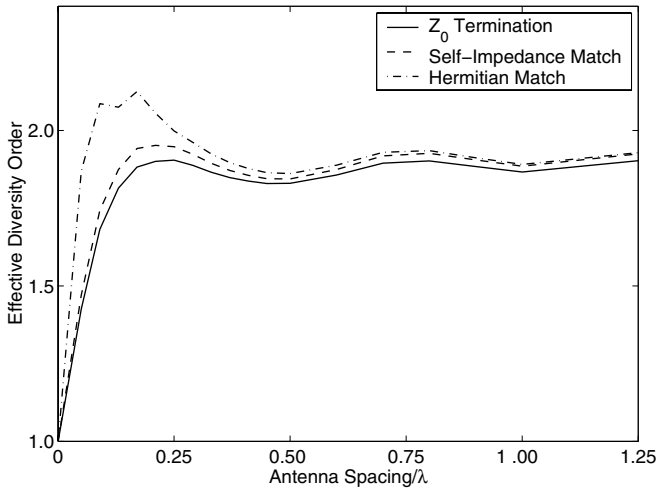

Fig. 4. Plot of effective diversity order as a function of antenna spacing for two coupled dipole antennas terminated with various loads. Correlations are computed from Monte Carlo simulations using a statistical path-based propagation model.

Finally, Figure 4 shows the diversity order as a function of spacing for when the channel is obtained using a statistical path-based channel model [11]. This model, which provides the angles and times of arrival for each individual multipath, structures these arrivals as clusters in space and time. In the simulations, 5000 channel realizations are used to estimate the covariance matrix $\overline{\overline{R}}_S$ for each antenna separation. While there certainly are some slight differences between the results in Figures 3 and 4, the main conclusions obtained from this more practical example are the same as those drawn from the more simplistic, previous computation. Note that one explanation for this similarity is that when 5000 channels are considered, the statistical distribution of the arrival angles tends to be uniform despite the clustered nature of a single realization.

V. Conclusion

This paper has presented a new analysis of multi-port matching networks, applicable to the mitigation of mutual coupling in compact antenna arrays. The framework leads to relatively straightforward expressions for the covariance matrix of signals received at the antenna terminations. These results were used in conjunction with electromagnetic analysis of coupled dipole antennas to demonstrate the potential diversity benefit offered by two-element arrays for different possible termination conditions. The results revealed that for close antenna spacing as might be encountered on portable devices, proper matching plays a noticeable role in determining the system performance. Perhaps more importantly, this framework provides a comprehensive analysis tool for characterizing and analyzing the performance of arbitrary coupled antenna systems, including all three relevant aspects of radiation pattern, mutual impedance, and antenna termination.

Acknowledgments: This work was supported by the National Science Foundation under Wireless Initiative Grant CCR 99-79452 and Information Technology Research Grant CCR-0081476.

References

[1] W. C. Jakes, *Microwave Mobile Communications*. IEEE Press, 1993.

[2] K. Boyle, "Radiation patterns and correlation of closely spaced linear antennas," *IEEE Trans. Antennas Propagat.*, vol. 50, pp. 1162–1165, Aug. 2002.

[3] S. C. K. Ko and R. D. Murch, "Compact integrated diversity antenna for wireless communications," *IEEE Trans. Antennas Propagat.*, vol. 49, pp. 954–960, Jun. 2001.

[4] M. A. Jensen and Y. Rahmat-Samii, "Performance analysis of antennas for hand-held transceivers using FDTD," *IEEE Trans. Antennas Propagat.*, vol. 42, pp. 1106–1113, Aug. 1994.

[5] J. Luo, J. R. Zeidler, and S. McLaughlin, "Performance analysis of compact antenna arrays with MRC in correlated Nakagami fading channels," *IEEE Transactions on Vehicular Technology*, vol. 50, pp. 267–277, Jan. 2001. [Online]. Available: http://www.ieeexplore.ieee.org/iel5/25/19842/00917940.pdf?isNumber=19842

[6] T. Svantesson and A. Ranheim, "Mutual coupling effects on the capacity of multielement antenna systems," in *IEEE ICASSP'2001*, vol. 4, Salt Lake City, UT, May 7-11 2001, pp. 2485–2488. [Online]. Available: http://www.ieeexplore.ieee.org/iel5/7486/20357/00940505.pdf?isNumber=20357

[7] O. Nørklit, P. D. Teal, and R. G. Vaughan, "Measurement and evaluation of multi-antenna handsets in indoor mobile communication," *IEEE Trans. Antennas Propagat.*, vol. 49, pp. 429–437, Mar. 2001.

[8] R. G. Vaughan and J. B. Andersen, "Antenna diversity in mobile communications," *IEEE Trans. Veh. Technol.*, vol. VT-36, pp. 147–172, Nov. 1987.

[9] R. G. Vaughan and N. L. Scott, "Closely spaced monopoles for mobile communications," *Radio Science*, vol. 28, pp. 1259–1266, Nov.-Dec. 1993.

[10] D. M. Pozar, *Microwave Engineering*. John Wiley & Sons, 1998.

[11] J. W. Wallace and M. A. Jensen, "Modeling the indoor MIMO wireless channel," *IEEE Trans. Antennas Propag.*, vol. 50, pp. 591–599, May 2002.

[12] A. C. Ludwig, "Wire-grid modelling of surfaces," *IEEE Trans. Antennas Propagat.*, vol. AP-35, pp. 1045–1048, Sep. 1987.